International Journal of Bifurcation and Chaos
© World Scientific Publishing Company

arXiv:1206.0789v1 [nlin.AO] 4 Jun 2012

Synchronization of coupled neural oscillators with heterogeneous delays

Anastasiia Panchuk
Institute of Mathematics, National Academy of Sciences of Ukraine, Kyiv, Ukraine

David P. Rosin
Institut für Theoretische Physik, Technische Universität Berlin, Hardenbergstraße 36, 10623 Berlin, Germany

Philipp Hövel
Institut für Theoretische Physik, Technische Universität Berlin, Hardenbergstraße 36, 10623 Berlin, Germany
Bernstein Center for Computational Neuroscience, Humboldt-Universität zu Berlin, Philippstraße 13, 10115 Berlin, Germany

Eckehard Schöll
Institut für Theoretische Physik, Technische Universität Berlin, Hardenbergstraße 36, 10623 Berlin, Germany, schoell@physik.tu-berlin.de

Received (to be inserted by publisher)

We investigate the effects of heterogeneous delays in the coupling of two excitable neural systems. Depending upon the coupling strengths and the time delays in the mutual and self-coupling, the compound system exhibits different types of synchronized oscillations of variable period. We analyze this synchronization based on the interplay of the different time delays and support the numerical results by analytical findings. In addition, we elaborate on bursting-like dynamics with two competing timescales on the basis of the autocorrelation function.

Keywords: delayed coupling, neural oscillators, synchronization

1. Introduction

A plethora of synchronization phenomena has been found for coupled nonlinear oscillators in physical, chemical and biological systems [Pikovsky *et al.*, 2001; Boccaletti *et al.*, 2002; Mosekilde *et al.*, 2002; Balanov *et al.*, 2009; Zhang *et al.*, 2011]. Especially the interplay of synchronization and time delay in coupled systems has received much interest recently [Schöll & Schuster, 2008; Just *et al.*, 2010; Atay, 2010]. Delayed coupling plays also a crucial role in the case of oscillation death [Choe *et al.*, 2007; Zou & Zhan, 2009; Zou *et al.*, 2012] and adaptive control schemes with delayed feedback applied to both chaotic [Wang *et al.*, 2010b; Lehnert *et al.*, 2011b] and non-chaotic systems [Selivanov *et al.*, 2012]. Previous studies involved networks of a large number of elements [Atay *et al.*, 2004; Dhamala *et al.*, 2004; Kinzel *et al.*, 2009; Choe *et al.*, 2010; Zigzag *et al.*, 2009; Englert *et al.*, 2010; Batista *et al.*, 2010; Kanter *et al.*, 2011; Flunkert & Schöll, 2012] as well as simple recurring substructures consisting of a few systems only, so-called *network motifs* [Hauschildt *et al.*, 2006; Choe *et al.*, 2007; D'Huys *et al.*, 2008; Hövel *et al.*, 2010a; Fiedler *et al.*,

2010; Flunkert *et al.*, 2009; Brandstetter *et al.*, 2010; D'Huys *et al.*, 2011; Hicke *et al.*, 2011; Kyrychko *et al.*, 2011; Adhikari *et al.*, 2011]. Considering the dynamics on networks with delay, the local elements can be either time-continuous or time-discrete as for iterated maps [Wang *et al.*, 2008a, 2009b]. In addition, a number of universal model-independent results have been obtained [Flunkert *et al.*, 2010; Heiligenthal *et al.*, 2011].

Synchronous dynamical patterns play also an important role in neuroscience [Rossoni *et al.*, 2005; Wang & Lu, 2005; Hauptmann *et al.*, 2007; Masoller *et al.*, 2008; Wang *et al.*, 2008b, 2009a; Masoller *et al.*, 2009; Senthilkumar *et al.*, 2009; Liang *et al.*, 2009; Lehnert *et al.*, 2011a; Popovych *et al.*, 2011], where on the one hand they can be observed in ensembles of neurons as pathological states like migraine, Parkinson's disease, or epilepsy. On the other hand synchronization can also be beneficial for recognition, learning, or neural information processing. Obviously the signal transmission between neurons in different brain areas is not instantaneous. Thus non-zero transmission times have to be taken into account as crucial quantities that influence the dynamics of individual neurons to a large extent. Consequently effects due to time delays have attracted more and more attention in the studies of neural networks [Rossoni *et al.*, 2005; Hauptmann *et al.*, 2007; Masoller *et al.*, 2008; Friedrich & Kinzel, 2009; Wang *et al.*, 2010a, 2011a; Lehnert *et al.*, 2011a; Kanter *et al.*, 2011; Wang *et al.*, 2011b] and particularly in motifs of two coupled neurons [Schöll *et al.*, 2009; Dahlem *et al.*, 2009; Hövel *et al.*, 2010a; Brandstetter *et al.*, 2010; Hövel *et al.*, 2009, 2010b]. The latter can be seen as the smallest entity in a larger network. Interestingly, phenomena observed in this area of research show a strong similarity with recent findings in optoelectronic oscillators [Rosin *et al.*, 2011].

Most previous works have assumed equal delay times in all connections. The focus of this paper, however, is on heterogeneous delays, which introduce additional timescales to the compound system. For this we consider a simple example of a network motif [Hauschildt *et al.*, 2006; Dahlem *et al.*, 2009; Panchuk *et al.*, 2009; Hövel *et al.*, 2010a], i.e., two delay-coupled neurons with delayed self-feedback, and we assume all delay times to be different. This configuration might as well be understood as two effective populations of larger clusters of neurons with delayed internal and mutual connections [Vicente *et al.*, 2008].

The rest of this paper is organized as follows: Section 2 introduces the neural model and the delay-coupling configurations. In Sec. 3, we study interaction involving identical self-coupling delays numerically and analytically. The results are extended to the case of nonidentical self-coupling delays in Sec. 4. Section 5 considers bursting dynamics. Finally, we close with a conclusion in Sec. 6.

2. Model

We study a compound system of two coupled neural elements each represented by a FitzHugh-Nagumo model [FitzHugh, 1961; Nagumo *et al.*, 1962]. The respective dynamic equations are paradigmatic for neural systems of type-II excitability, when periodic oscillations are generated in a Hopf bifurcation. We consider the case where the two elements are coupled such that each neural oscillator is subject to the delayed response from the other one. See Fig. 1 for a schematic diagram, where the time delays are denoted by τ_1^C and τ_2^C and C is the coupling strength. In addition, we take also delayed self-feedback [Pyragas, 1992] with a delay time τ_i^K, $i = 1, 2$ and feedback strength K into account.

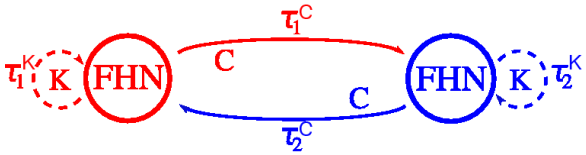


Fig. 1. Schematic diagram of two coupled neural elements including the parameters of the mutual coupling (time delays τ_1^C, τ_2^C and coupling strength C) and the self-feedback (time delays τ_1^K, τ_2^K and feedback gain K).

The two coupled FitzHugh-Nagumo systems are described by the following set of delay differential

equations:

$$\begin{aligned}
\varepsilon_1 \dot{x}_1 &= x_1 - \frac{x_1^3}{3} - y_1 + C\left[x_2\left(t-\tau_2^C\right) - x_1(t)\right] \\
&\quad + K\left[x_1\left(t-\tau_1^K\right) - x_1(t)\right] && \text{(1a)} \\
\dot{y}_1 &= x_1 + a && \text{(1b)} \\
\varepsilon_2 \dot{x}_2 &= x_2 - \frac{x_2^3}{3} - y_2 + C\left[x_1\left(t-\tau_1^C\right) - x_2(t)\right] \\
&\quad + K\left[x_2\left(t-\tau_2^K\right) - x_2(t)\right] && \text{(1c)} \\
\dot{y}_2 &= x_2 + a, && \text{(1d)}
\end{aligned}$$

where ε_i denotes the timescale ratio between the slow inhibitor variable y_i and the fast activator variable x_i $(i = 1, 2)$. The parameter a is known as threshold parameter. For $|a| > 1$, the uncoupled system operates in the excitable regime.

As it was shown in Ref. Panchuk *et al.* [2009], two coupled systems with asymmetric delay times τ_1^C, τ_2^C can be reduced to a system with symmetric delay times τ^C. The difference between τ_1^C and τ_2^C leads only to a phase shift between oscillator 1 and 2. Therefore, we assume them to be equal $\tau_1^C = \tau_2^C = \tau^C$ without loss of generality and Eqs. (1) can be rewritten as follows

$$\begin{aligned}
\varepsilon \dot{x}_1 &= x_1 - \frac{x_1^3}{3} - y_1 + C\left[x_2\left(t-\tau^C\right) - x_1(t)\right] \\
&\quad + K\left[x_1\left(t-\tau_1^K\right) - x_1(t)\right] && \text{(2a)} \\
\dot{y}_1 &= x_1 + a && \text{(2b)} \\
\varepsilon \dot{x}_2 &= x_2 - \frac{x_2^3}{3} - y_2 + C\left[x_1\left(t-\tau^C\right) - x_2(t)\right] \\
&\quad + K\left[x_2\left(t-\tau_2^K\right) - x_2(t)\right] && \text{(2c)} \\
\dot{y}_2 &= x_2 + a. && \text{(2d)}
\end{aligned}$$

Throughout this paper, we choose the following set of parameters, unless specified otherwise: $\varepsilon_1 = \varepsilon_2 = \varepsilon = 0.01$, $a = 1.3$, $\tau^C = 3$, and $C = 0.5$.

For $|a| > 1$, the fixed point is always linearly stable (cf. Ref. Panchuk *et al.* [2009]) and the system Eq. (2) shows various regular spiking and bursting patterns. Furthermore, several stable solutions can coexist for the same parameter values entailing high-level multi-stability.

Before exploring the interplay between three different delay times, namely the mutual coupling delay τ^C and two nonidentical self-coupling delays $\tau_1^K \neq \tau_2^K$ (Secs. 4 and 5), we will consider the case $\tau_1^K = \tau_2^K \equiv \tau^K$ in the next Section. Analytical conditions for coherent spiking will be derived and generalized in the subsequent sections.

3. Identical self-feedback delays

The dynamics of the compound system (2) is diverse and hence, we will first introduce a classification. For this purpose, we will use an approach based on the mean interspike interval (ISI) $\left\langle T_j^{(i)} \right\rangle \equiv T^{(i)}$, where $\left\{T_j^{(i)}\right\}_{j=1}^{N}$ is the set of N interspike intervals for the time series of the i-th neuron $(i = 1, 2)$ [Dahlem *et al.*, 2009; Schöll *et al.*, 2009]. A measure based on the ISI is a powerful tool to characterize regular, coherent spiking that is similar to a period-1 orbit. Therefore, we take the ISI values for those cases into account that have small standard deviation. Failure of such a measure, e.g., for bursting dynamics, will be discussed in later sections.

Figure 2 shows exemplary time series of coherent spiking for different values of K and τ^K, while the mutual coupling delay and strengths are fixed at $\tau^C = 3$ and $C = 0.5$, respectively. The parameters are chosen as $(K = 0.05, \tau^K = 3)$, $(K = 0.5, \tau^K = 3)$, $(K = 0.5, \tau^K = 2)$, and $(K = 0.5, \tau^K = 4)$ in panels (a)-(d), respectively. All these combinations of τ^K and K exhibit coherent spiking, where the ISI is constant,

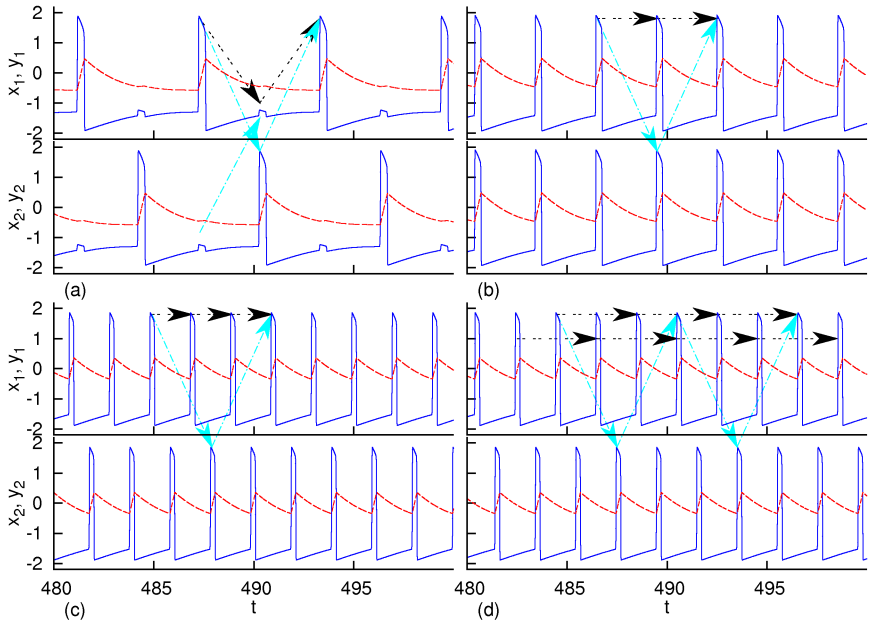


Fig. 2. Time series of Eqs. (2) for identical self-feedback delays $\tau_1^K = \tau_2^K = \tau^K$. The activator x_i and inhibitor y_i are shown by blue (full) and red (dashed) curves, respectively. The parameters are chosen as (a) $K = 0.05, \tau^K = 3$, (b) $K = 0.5, \tau^K = 3$, (c) $K = 0.5, \tau^K = 2$, and (d) $K = 0.5, \tau^K = 4$. The black and light blue arrows show excitations due to self-feedback and mutual feedback, respectively. Other parameters: $\varepsilon = 0.01$, $a = 1.3$, $\tau^C = 3$, and $C = 0.5$.

hence the standard deviation vanishes. Since the fixed point in the individual subsystems is stable in the excitable regime, we choose initial conditions such that only one subsystem is located in the fixed point whereas the other is subjected to a one-time-only excitation. This initial excitation eventually remains in the compound system due to the delayed coupling.

Comparing Figs. 2(a) and (b), one can see that small self-feedback gains, e.g., $K = 0.05$ in Fig. 2(a), are not able to trigger superthreshold excitations. Only subthreshold oscillations occur after times τ^K as indicated by a black arrow in Figs. 2(a). In the following, we will derive analytical conditions for the delay times τ^K and τ^C such that regular, superthreshold spiking occurs.

If the coupling strengths K and C are large enough, a spike at time t in one system will induce spikes at times $t + \tau^C$ in the other system (see light blue arrows) and $t + \tau^K$ in the first system (black arrows) by mutual coupling and self-feedback, respectively. The spike in the second system returns after a round-trip time $2\tau^C$. Thus, we have excitation events at times $t + \tau^K$ and $t + 2\tau^C$ in each subsystem. The spikes induced by these two sources of excitation become coherent, i.e., in resonance, when the delay time due to a round trip to the other system and back again, i.e., $2\tau^C$ matches with the self-coupling delay τ^K. The same argument holds for integer multiples of τ^K and $2\tau^C$, leading to the following condition

$$N^K \tau^K = N^C 2\tau^C, \tag{3}$$

with integer numbers N^K and N^C.

Using this notation, Fig. 2 displays some combinations of N^K and N^C for coherently spiking states. Panels (a) and (b) refer to time delays $\tau_K = 3 = \tau_C$ with $N^C = 1$ and $N^K = 2$. While panel (a) shows subthreshold oscillations after τ^K and superthreshold oscillations only after $2\tau^C$, panel (b) corresponds to a resonance yielding only fully pronounced, regular oscillations. Other values of the self-feedback delay, e.g., $\tau_K = 2$ and $\tau_K = 4$, result in different combinations of N^K and N^C. See, for instance, panels (c) and (d) that correspond to $N^K = 3$, $N^C = 1$, and $N^K = 3$, $N^C = 2$, respectively. For superthreshold oscillations, Eq. (3) yields the following condition for coherent spiking:

$$\tau^K = \frac{2\tau^C N^C}{N^K}. \tag{4}$$

The corresponding ISIs are given by

$$T = \frac{2\tau^C}{N^K} = \frac{\tau^K}{N^C} \tag{5}$$

with minimal integer numbers N^K, N^C, i.e., the fraction N^K/N^C is irreducible.

Equation (5) reflects the resonance condition (3): N^K spikes are induced by self-coupling during the round trip time $2\tau^C$ of the mutual coupling. See Figs. 2(b)-(d). Figure 3 compares this analytical result to the numerical simulation. The green bars (positive T) show the numerically simulated ISI in dependence on τ^K for standard deviations smaller than 0.01. The other parameters are fixed at $K = 0.5$, $C = 0.5$, and $\tau^C = 3$. For larger standard deviations the spiking is not coherent anymore. The red bars (negative T, i.e., inverted to facilitate comparison) show the analytically calculated delay times τ^K for which spiking occurs, and the value of the associated ISI using Eqs. (4), (5) and (9), (10). The latter describe the width of the resonance bars and will be derived later. It can be seen that the analytic results are in good agreement with the time delay τ^K, for which coherent spiking is found with the corresponding ISI T in the numerical simulation. Due to finite numerical accuracy, not all analytically possible ISI are detected in the time series. For large integers N^C and N^K, coherent spiking does not occur.

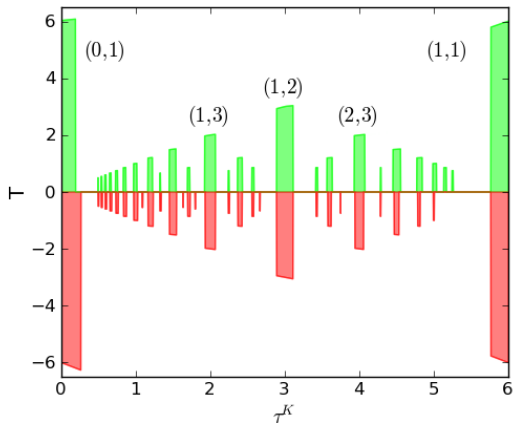


Fig. 3. Period of possible ISIs of coherent spiking in dependence on τ_K for $K = 0.5$ and $C = 0.5$. The mutual time delay is fixed at $\tau^C = 3$. Green: numerical simulation; red inverted values: analytical calculation using Eqs. (4), (5) and Eqs. (9), (10). The parentheses refer to some exemplary values (N^C, N^K). Other parameters as in Fig. 2.

It is possible to derive a condition concerning a possible phase shift of spikes in the activator variables x_1 and x_2 in the regime of coherent spiking as displayed, for instance, by Figs. 2(c) and (d). If we find integers $\widetilde{N}^K$ and N^C with

$$\widetilde{N}^K \tau^K = N^C \tau^C, \tag{6}$$

spikes in the first and second oscillator coincide. Thus for $\widetilde{N}^K = N^K/2 \in \mathbb{N}$ leading to N^K even, there is no phase difference, i.e., we observe in-phase oscillations. Otherwise, for odd N^K, the phase shift is π corresponding to anti-phase oscillations. Using Eq. (4) we are able to predict for which values of τ^K and τ^C anti-phase oscillations occur.

In order to introduce some helpful notation for the following derivation, Figs. 4(a) and 4(b) display a time series and the respective phase portrait of a typical behavior of the neural system under consideration. A full excursion in phase space consists of a round trip from A through points B, C, and D back to A. The times for the transitions from A to B and from C to D are negligible, since the activator variables x_1 change much faster than the inhibitors y_1, due to timescale separation $\varepsilon \ll 1$. The transition from B to C happens close to the right slow branch of the cubic nullcline during a fixed firing time $T_f = T_{B\to C}$. In an earlier publication [Schöll *et al.*, 2009] we derived the following analytical approximation for the firing

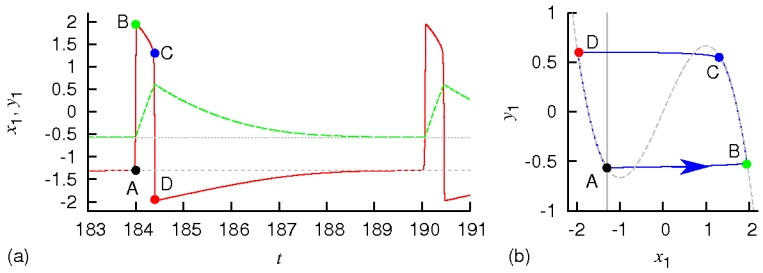


Fig. 4. (a) Time series and (b) phase portrait of a numerical solution of Eq. (2) for $K = 0$, $C = 0.5$, and $\tau^C = 3$. Other parameters as in Fig. 2.

time T_f

$$T_f = \int_B^C \frac{dx_1}{\dot{x}_1} = \int_B^C \frac{1 - x_1^2}{x_1 + a} dx_1 \tag{7a}$$

$$= \left(a^2 - 1\right) \ln \frac{a+2}{a+1} - a + \frac{3}{2} \tag{7b}$$

with $x_1 = 2$ and $x_1 = 1$ as an approximation for points B and C, respectively. Thus, we obtain a value of $T_f \approx 0.45$ for $a = 1.3$. Note that this approximation is valid for parameter values of a close to 1. For an improved estimate of T_f further away from the bifurcation point, one can use the position of the fixed point, i.e., intersection of the nullclines. For details see Appendix 1. For the final transition from D to A there remains the time $T_{D\to A} = T - T_f$, which will be considered later in this Section.

In Fig. 3 one sees that each area of coherent spiking has a certain width. In the following we will derive an expression for the width $\Delta\tau^K$ of these coherence tongues by using the quantity T_f. For this, we will soften the condition (3) to within a certain tolerance: If the time shift $|N^K\tau^K - N^C 2\tau^C|$ is smaller than half the firing time $T_f/2$, spiking still occurs even though Eq. (3) is only approximately fulfilled. This leads to the following relation

$$\left| N^K \left(\tau^K \pm \frac{\Delta\tau^K}{2} \right) - N^C 2\tau^C \right| \leq \frac{T_f}{2}. \tag{8}$$

Here $\Delta\tau^K$, i.e., the width of the coherence tongues, acts as tolerance in the timing of the incoming excitations. Equation (8) yields an upper bound for $\Delta\tau^K$

$$\left|\Delta\tau^K\right| \leq \frac{T_f + 2\left|N^C 2\tau^C - N^K\tau^K\right|}{N^K}. \tag{9}$$

Recalling condition (3), this simplifies to

$$\left|\Delta\tau^K\right| \leq \frac{T_f}{N^K}. \tag{10}$$

For a better analysis of the behavior of the compound system, it is helpful to investigate the ISI. Figure 5 shows the ISI as color code in the $\left(K, \tau^K\right)$-plane for fixed $\tau^C = 3$. Note that only spiking with an ISI standard deviation smaller than 0.01 is depicted. In the white region the standard deviation of the ISIs is large. Thus, white color marks the region, where no coherent spiking occurs. The horizontal lines correspond to delays τ^K in the self-coupling which are in resonance to τ^C. Some combinations of K and τ^K are marked by black dots (a) - (d) referring to the time series in Fig. 2.

The bright yellow region at small K and τ^K values refers to a regime, where oscillations with $T = 2\tau^C = 6$ dominate the dynamics due to mutual coupling, while the self-coupling leads only to subthreshold oscillations. In these cases, the self-coupling is too weak or too fast, i.e., small K or small τ^K, respectively, to initiate additional spikes. Compare also Fig. 2(a). The black region for large K and small τ^K corresponds to oscillation death due to the refractory phase of the neural oscillator [Schöll *et al.*, 2009]. There the subsystem is not susceptible to an incoming activating signal.

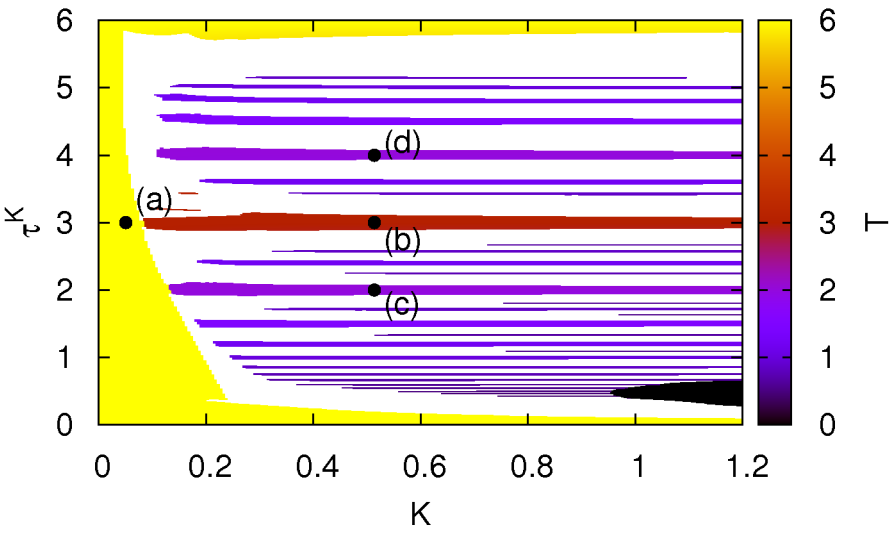


Fig. 5. Interspike intervals of the spiking state obtained from numerical simulations in dependence on K and τ^K with fixed $\tau^C = 3$ and $C = 0.5$. The values marked by (a) to (d) refer to time series displayed in Fig. 2. Other parameters as in Fig. 2. A spike is considered as an excursion in phase space with $x_1 > 0$.

One can also calculate analytically the threshold at which the coherent spiking with $T = 2\tau^C$ ceases, i.e., the border between the bright yellow and the white regime in Fig. 5. At this boundary, self-coupling becomes strong enough to excite superthreshold spikes. To calculate an analogous boundary in Fig. 6, we set $K = 0$ and vary C and τ^C and extend the analytic result later to nonzero self-coupling strength K to calculate the boundary in Fig. 5. Using the notation introduced above, the transition from D to A in Fig. 4 completes a full excursion. This last transition happens during a time interval $T_{D\to A} = T - T_f$. At this stage of the spike, the neural system is susceptible for the next excitation. For long periods T, the system relaxes to the fixed point x_{FP}. For periods T used in this paper, however, the next excitation happens already at an earlier point A $= (x_{1,end}, y_{1,end})$. An analytical estimate for $T_f = T_{B\to C}$ is given above, see Eq. (7b). We can derive a similar formula for $T_{D\to A}$

$$T_{D\to A} = \int_D^{x_{1,end}} \frac{1 - x_1^2}{x_1 + a} dx_1. \tag{11}$$

If the system exhibits spikes with a period $T = 2\tau^C$, we have $T_{D\to A} = 2\tau^C - T_f$. Using this value, Eq. (11) yields an implicit expression for $x_{1,end}$

$$x_{1,end} = (a-2)\exp\left(\frac{p - 2\tau^C + T_f}{a^2 - 1}\right) - a \tag{12}$$

with the abbreviation $p = a(2 + x_{1,end}) + 2 - x_{1,end}^2/2$ that depends upon $x_{1,end}$. Since the relaxation from D to A follows closely the cubic y-nullcline, we can calculate a value for $y_{1,end}$ as follows:

$$y_{1,end} = x_{1,end} - \frac{x_{1,end}^3}{3}. \tag{13}$$

The mutual coupling ($K = 0$, $C \neq 0$) serves as an input in Eqs. (2a) and (2c). Thus, it leads to a temporary, vertical shift of the cubic y-nullcline. If the minimum $(x_{1,min}, y_{1,min})$ of this dynamic y-nullcline, which includes input from the coupled system, is shifted beyond the point A$= (x_{1,end}, y_{1,end})$, a spike is

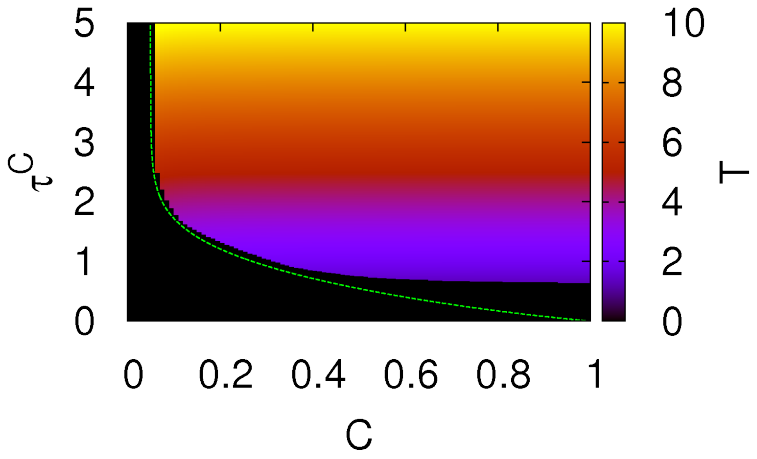


Fig. 6. Interspike intervals T of spikes in dependence on C and τ^C for vanishing self-coupling ($K = 0$). The dashed green curve refers to an analytical approximation of the excitation threshold for $x_2(t-\tau^C) = 1$ in Eq. (15b). Other parameters as in Fig. 2.

triggered. The equation for the dynamic y-nullcline (for $K = 0$) is given by

$$y_1 = x_1 + \frac{x_1^3}{3} + C\left[(x_2(t-\tau^C) - x_1\right], \tag{14}$$

which depends on the delayed activator variable $x_2(t-\tau^C)$ that eventually induces the next spike. The minimum of this nullcline can easily be calculated as

$$x_{1,min} = -\sqrt{1-C} \tag{15a}$$

$$y_{1,min} = x_{1,min} - \frac{x_{1,min}^3}{3} + C\left[x_2(t-\tau^C) - x_{1,min}\right]. \tag{15b}$$

Finally, the condition $y_{1,end} = y_{1,min}$ determines the boundary between coherent spiking and the quiescent state. Note that the delayed response $x_2(t-\tau^C)$ in Eq. (15b) remains to be chosen.

The analytically calculated excitation threshold is shown in Fig. 6 as a dashed green curve for $x_2(t-\tau^C) = 1$. This value is motivated by the assumption that (x_2, y_2) is located at point C in Fig. 4(b) at time $t-\tau^C$. The ISI is depicted in color code. The black region refers to the quiescent state.

Following the derivation described above, one can also calculate the excitation threshold for $K \neq 0$ and fixed mutual coupling parameters C, τ^C in a similar way. For this, Eq. (14) needs to be extended as follows:

$$\begin{aligned} y_1 = x_1 + \frac{x_1^3}{3} + C\left[(x_2(t-\tau^C) - x_1\right] \\ - K\left[(x_2(t-\tau^K) - x_1\right], \end{aligned} \tag{16}$$

Similarly Eqs. (15) become

$$x_{1,min} = -\sqrt{1-C-K} \tag{17a}$$

$$\begin{aligned} y_{1,min} = x_{1,min} - \frac{x_{1,min}^3}{3} + C\left[x_2(t-\tau^C) - x_{1,min}\right] \\ + K\left[x_2(t-\tau^K) - x_{1,min}\right]. \end{aligned} \tag{17b}$$

Here one has to choose appropriate values for $x_2(t-\tau^C)$ and $x_2(t-\tau^K)$.

Now we assume that the self-coupling delay τ^K sets the period of the regular spiking leading to $T_{D\to A} = \tau^K - T_f$. Accordingly, the time $2\tau^C$ in Eq. (12) of $x_{1,min}$ has to be replaced by τ^K. Then the condition derived from $y_{1,end} = y_{1,min}$, i.e., Eqs. (13) and (17b), and Eqs. (5) and (10) for the ISI lead

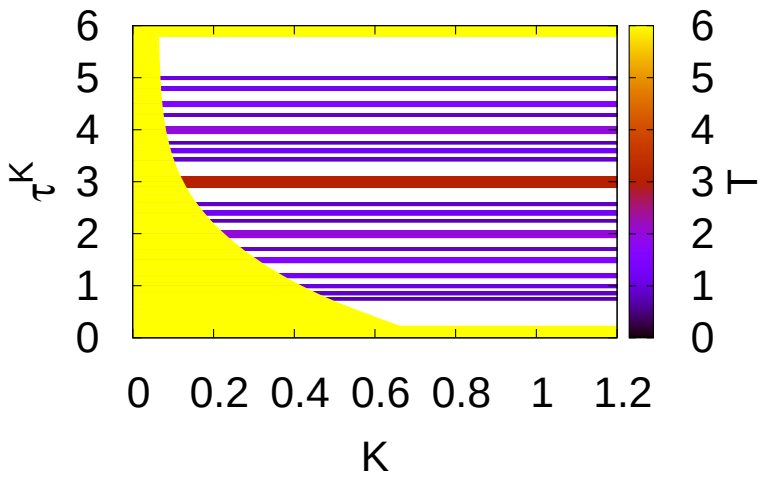


Fig. 7. Analytical calculation of the interspike intervals of the spiking state with $\tau^C = 3$ and $C = 0.5$ using Eqs. (4), (5) and (9), (10). The delayed values $x_2(t-\tau^C)$ and $x_2(t-\tau^K)$ are chosen as -1.3 and 2. Other parameters as in Fig. 2.

to Fig. 7 that displays the analytically calculated ISIs. The delayed values $x_2(t-\tau^C)$ and $x_2(t-\tau^K)$ are chosen as -1.3 and 2, i.e., as points A and B in Fig. 4(b), respectively. This figure is in good agreement with Fig. 5, which shows the numerically simulated ISIs. Not only the location of the coherence tongues are reproduced by the analytical formulas, but also their widths are in good agreement.

4. Nonidentical self-coupling delays

As one can see from the previous analysis, the dynamics of system (2) exhibits a variety of different solutions already for the simplifying restriction $\tau_1^K = \tau_2^K = \tau^K$. In what follows we will consider $\tau_1^K \neq \tau_2^K$, in which case one can expect even richer dynamics. The initial conditions are kept as before, i.e., one subsystem is initialized with a one-time excitation.

In Fig. 8, ISI diagrams in the $\left(K, \tau_1^K\right)$-parameter space are plotted for $C = 0.5$, $\tau^C = 3$, and $\tau_2^K = 2$ in color code. Again, white areas correspond to those solutions for which the ISI standard deviation is larger than a threshold value set to 0.02. The colored areas refer to parameters, for which coherent oscillations similar to a period-1 orbit appear, associated with a single spike during one period.

Comparing Fig. 8 with Fig. 5, i.e., the case of equal self-feedback delays, one finds common features like resonances or a boundary of the $T = 2\tau^C$ periodic dynamics at small K. A closer look, however, reveals also distinct differences. Some of the parameter regions of coherent spiking appear as tongues at specific ratios of the delays. This time, the regions with $\tau_1^K = \tau_2^K$ and $\tau_1^K = 2\tau_2^K$ are more pronounced than for $\tau_1^K = \tau^C$. The reason is that now the fixed self-coupling delay τ_2^K sets the basic timescale.

Using the same argument as in Sec. 3 we can derive resonance conditions similar to Eq. (3). Namely, we need to require resonance for all pairs of the coupling delays: (i) τ_1^K and $2\tau^C$, (ii) τ_2^K and $2\tau^C$, as well as (iii) τ_1^K and τ_2^K. The first two assumptions yield, as before,

$$N_1^C 2\tau^C = N_1^K \tau_1^K \tag{18}$$

with irreducible integers N_1^C/N_1^K, and

$$N_2^C 2\tau^C = N_2^K \tau_2^K \tag{19}$$

with irreducible integers N_2^C/N_2^K. Furthermore, Eq. (18) divided by Eq. (19) immediately leads to

$$N_1 \tau_1^K = N_2 \tau_2^K \tag{20}$$

with $N_1 = N_2^C N_1^K/d$ and $N_2 = N_2^C N_1^K/d$, where d is the greatest common divisor of $N_2^C N_1^K$ and $N_2^C N_1^K$. Therefore, if the relations (18) and (19) are satisfied, system (2) performs coherent spiking. Note that for

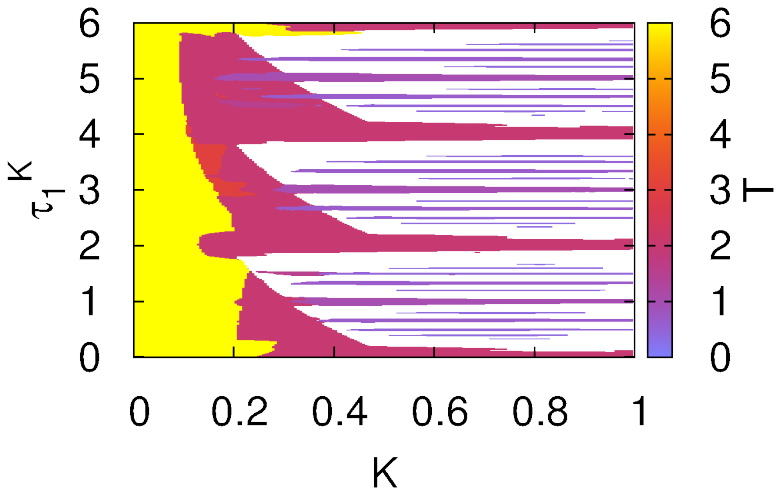


Fig. 8. Interspike intervals T in the $\left(K, \tau_1^K\right)$-plane with $\tau^C = 3, \tau_2^K = 2$ as color code. Only solutions with an ISI standard deviation smaller than 0.02 are shown. Other parameters as in Fig. 2.

any three rational numbers τ^C, τ_1^K, and τ_2^K there always exist corresponding integers N_1^C, N_1^K, N_2^C, N_2^K, N_1 and N_2, for which the Eqs. (18)-(20) hold.

The period of the coherent solution is also obtained by analogy with the previous case. First, we find from Eqs. (18) and (19)

$$T_1 = \frac{2\tau^C}{N_1^K} = \frac{\tau_1^K}{N_1^C}, \tag{21}$$

$$T_2 = \frac{2\tau^C}{N_2^K} = \frac{\tau_2^K}{N_2^C}. \tag{22}$$

Finally using Eq. (20) we have

$$T_3 = \frac{\tau_1^K}{N_1} = \frac{\tau_2^K}{N_2}. \tag{23}$$

Thus, the estimated period is

$$T = \min\{T_1, T_2, T_3\}. \tag{24}$$

As a consequence, if N_1^K, N_2^K, N^C, N_1, and N_2 are large, the estimated oscillation period becomes small. Then the coherent solution cannot be realized due to the refractory phase of the neural subsystems.

In order to determine the width of the areas for coherent spiking in the $\left(K, \tau_1^K\right)$-plane, we use a similar reasoning as before. From Eqs. (18) and (20) we get

$$\left| N_1^K \left(\tau_1^K \pm \frac{\Delta\tau_1^K}{2} \right) - N^C 2\tau^C \right| \leq \frac{T_f}{2} \tag{25}$$

and

$$\left| N_1 \left(\tau_1^K \pm \frac{\Delta\tau_1^K}{2} \right) - N_2 \tau_2^K \right| \leq \frac{T_f}{2}, \tag{26}$$

respectively. As a result, the width of the regular spiking regime simplifies to

$$\left|\Delta\tau_1^K\right| \leq \min\left\{ \frac{T_f}{N_1^K}, \frac{T_f}{N_1} \right\}. \tag{27}$$

Figure 9 shows the analytical estimate for the tongues of coherent spiking corresponding to Eqs. (18) and (19). The region for the solution of period $T \approx 2\tau^C$ is obtained numerically at small feedback gains K. There is a good correspondence to Fig. 8, however, some approximated regions for solutions with small

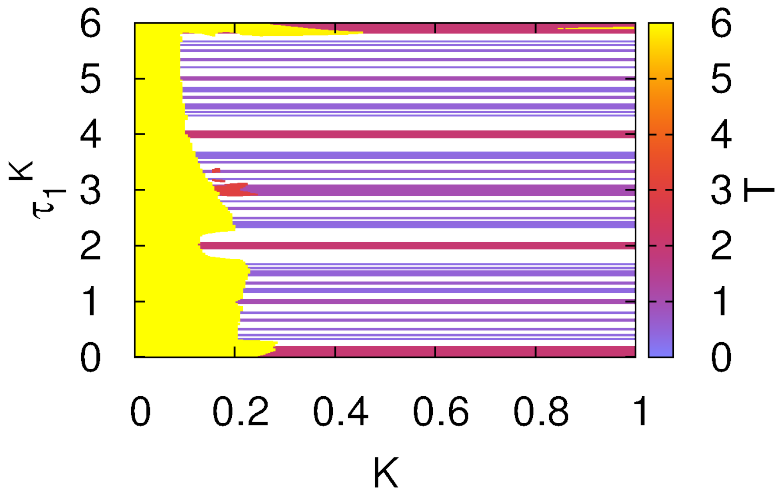


Fig. 9. Analytical approximation of tongues for coherent spiking with period less than $2\tau^C$ in the $\left(K, \tau_1^K\right)$-plane ($\tau^C = 3, \tau_2^K = 2$). The firing time T_f is set to 0.38 (see Appendix 1). The yellow region for the solution of period $2\tau^C$ at small K is calculated numerically. Other parameters as in Fig. 2.

periods are wider than the simulated ones. The reason is that the approximation for the firing time T_f, given by Eq. (A.1), is still too rough. For small periods, the solution looks as exemplarily depicted in Fig. 10, and the derivation for T_f does not hold anymore.

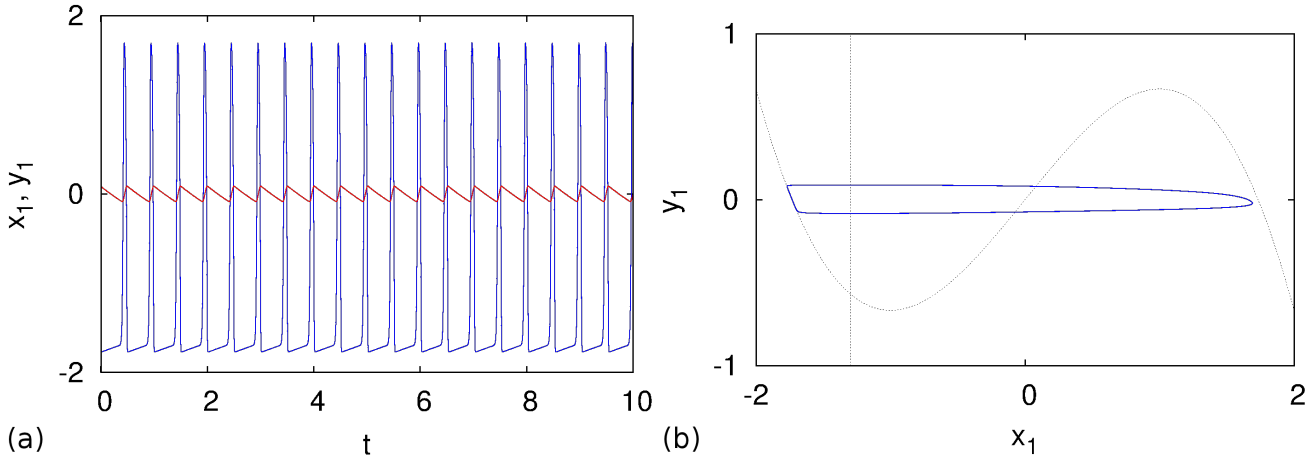


Fig. 10. Time series and phase portrait of the first subsystem variables x_1 and y_1 as blue and red curves for the periodic solution with period $T \approx 0.5$. Self-coupling parameters: $K = 0.5, \tau_1^K = 0.5, \tau_2^K = 2$. Other parameters as in Fig. 2.

As a generalization of our previous analytical approach, we can derive a relation between all three delay times in general form. Provided that the parameters C and K are large enough to yield superthreshold excitation, the spike of the first neuron at time t will induce spikes at times $t+\tau_1^K$ and $t+2\tau^C$. Similarly the second neuron will spike at time $t+\tau^C$, as well as at times $t+\tau^C+\tau_2^K$, $t+\tau^C+2\tau_2^K$, $t+\tau^C+3\tau_2^K, \ldots$. Thus, the first subsystem will get also excitation impulses at times $t+2\tau^C+\tau_2^K$, $t+2\tau^C+2\tau_2^K$, $t+2\tau^C+3\tau_2^K$, and so on. From this we get

$$m_1\tau_1^K = l_1(2\tau^C + n_1\tau_2^K), \tag{28}$$

where l_1, m_1, n_1 are arbitrary positive integers. The same discussion is applicable for the second subsystem, and therefore we can also write down the symmetric condition

$$n_2\tau_2^K = l_2(2\tau^C + m_2\tau_1^K) \tag{29}$$

with positive integers l_2, m_2, n_2. Adding Eqs. (28) and (29) we derive

$$2(l_1 + l_2)\tau^C = (m_1 - l_2 m_2)\tau_1^K + (n_2 - l_1 n_1)\tau_2^K.$$

Denoting $\tilde{l} = 2(l_1 + l_2)/d$, $\tilde{m} = (m_1 - l_2 m_2)/d$, and $\tilde{n} = (n_2 - l_1 n_1)/d$, where d is the greatest common divisor of the three numbers $2(l_1 + l_2)$, $m_1 - l_2 m_2$, and $n_2 - l_1 n_1$, we get

$$\tilde{l}\tau^C = \tilde{m}\tau_1^K + \tilde{n}\tau_2^K \tag{30}$$

with integers $\tilde{l} > 0$, and $\tilde{m}$, $\tilde{n}$ being of any sign. Note that Eq. (30) can also be obtained directly from adding or subtracting Eqs. (18) and (19).

At last, by moving all the terms onto one side of the equation and relabeling, Eq. (30) can be rewritten in the general form:

$$l\tau^C + m\tau_1^K + n\tau_2^K = 0, \tag{31}$$

where l, m, n are arbitrary integers of any sign. It should be mentioned that the relation similar to Eq. (31) was obtained in Ref. Zigzag *et al.* [2009] for a two-dimensional time-discrete system with several non-equal delays.

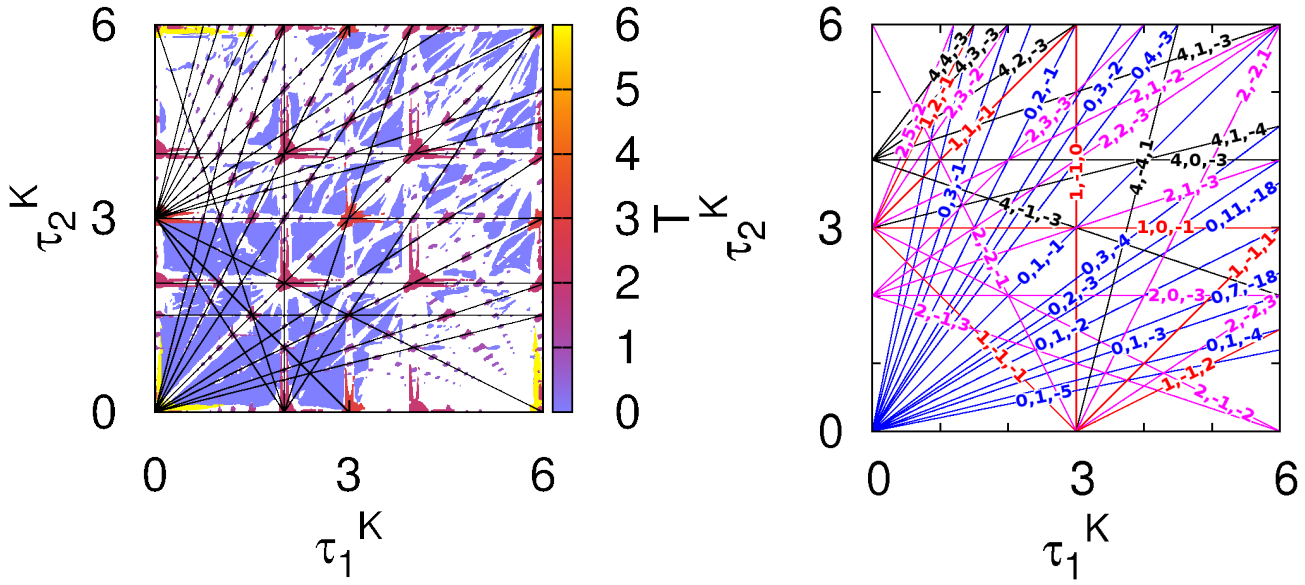


Fig. 11. (a) Interspike intervals T in the $\left(\tau_1^K, \tau_2^K\right)$-plane for $\tau^C = 3, K = 0.5$. The black lines are added according to Eq. (31); (b) resonance lines given by Eq. (31) including the integer values of l, m, and n. Other parameters as in Fig. 2.

If we fix τ^C, Eq. (31) defines different lines in the (τ_1^K, τ_2^K)-plane, depending on l, m, and n. Figure 11(a) visualizes multiple combinations as black lines on top of the ISI T shown in color code. The regions, in which periodic solutions were found numerically, accumulate along the lines that are given by Eq. (31). In Fig. 11(b) these analytically obtained conditions are separately shown including the values of l, m, and n. The analytical results are in excellent agreement with the numerical calculations.

5. Bursting and autocorrelation function

In Fig. 11(a) of the previous section, the lines obtained analytically from the resonance condition (31) agree very well with the numerical results on the ISI of regular spiking. However, the regions of periodic spiking fill only a part of the parameter plane. The ISI approach does not allow for an analysis of bursting-type solutions. There, the time series exhibits bunched spiking patterns and thus different timescales.

Therefore, we consider the autocorrelation function (ACF) $\Psi(s)$ as an alternative tool for the analysis of the coupled system dynamics [Hauschildt *et al.*, 2006]. The ACF $\Psi(s)$ of an arbitrary time series $x(t)$ is

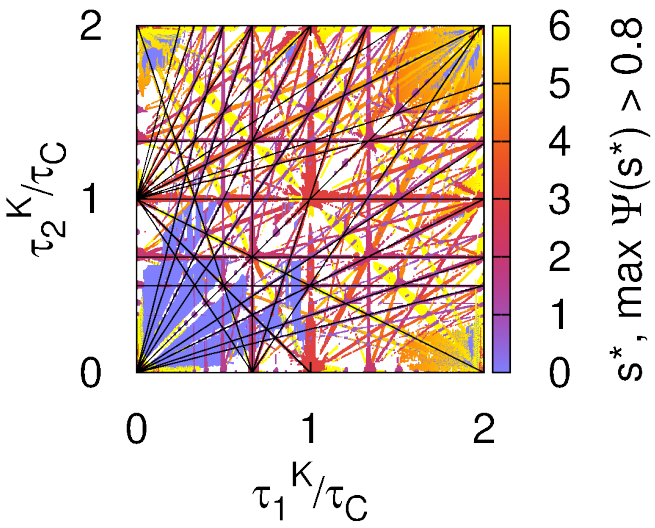


Fig. 12. Maxima of the autocorrelation function Ψ in the $\left(\tau_1^K, \tau_2^K\right)$-plane for $\tau^C = 3, K = 0.5$. The black lines lines are given by the Eq. (30). Other parameters as in Fig. 2.

defined as

$$\Psi(s) = \frac{1}{\sigma^2} \left\langle [x(t-s) - \langle x \rangle][x(t) - \langle x \rangle] \right\rangle , \tag{32}$$

where the averages $\langle \cdot \rangle$ are calculated over the whole simulated time interval. The value σ denotes the standard deviation of $x(t)$, i.e., $\sigma^2 = \left\langle [x(t) - \langle x \rangle]^2 \right\rangle$.

To determine whether a given solution shows quasi-periodic neural activity, we calculate the ACF $\Psi(s)$ of $x_1(t)$, which has several maxima. The first, trivial maximum is, obviously, obtained at $s = 0$ and equals 1. The second largest maximum marks the best coincidence between the original and the shifted time series, and is found for $s = s^*$, which characterizes the length of the repeated (periodic or quasi-periodic) pattern, and in case of periodic spiking equals the ISI.

The result of this alternative analysis based on the ACF is depicted in Fig. 12. In this figure, the resonances of Eq. (31) (Fig. 11(b)) are fully visible and well separated from each other, cf. the yellow and red areas in Fig. 12 that are missing in Fig. 11(a).

The ACF allows for investigation of both periodic and quasi-periodic behavior. Figure 13 shows time series and phase space projections for bursting-type solutions. Since the time series consists of repeated bunches of spikes, the mean interspike interval is no longer a good measure. This is due to two different timescales in the activator variables x_1 and x_2. To investigate this bursting-type behavior we use again the ACF analysis.

Figure 14(b) displays the ACF of the time series from Fig. 13. In Fig. 14(a) the time series for the first activator x_1 is shown again for convenience and Fig. 14(b) presents the ACF $\Psi(s)$. It can be seen that the ACF approaches unity for the second time – after the trivial perfect correlation at $s = 0$ – at a displacement of $s = s^* \approx 2.01$, which equals the repetition period of the bursting pattern. The bursts can also be resolved by the ACF as the fast oscillations. To conclude, the ACF enables to distinguish between inter-burst and intra-burst timescales.

6. Conclusion

We have investigated effects of heterogeneous time delays for mutual and self-coupling of a simple network motif that consists of two neural systems. This setup is realized by two delay-coupled elements of FitzHugh-Nagumo type, which is a paradigmatic model of neural interaction. The two subsystems operate in the excitable regime, and excitation occurs due to the incoming delayed signals via both mutual and self-coupling.

At first, we have considered identical self-coupling delays and analyzed the regular periodic dynamics

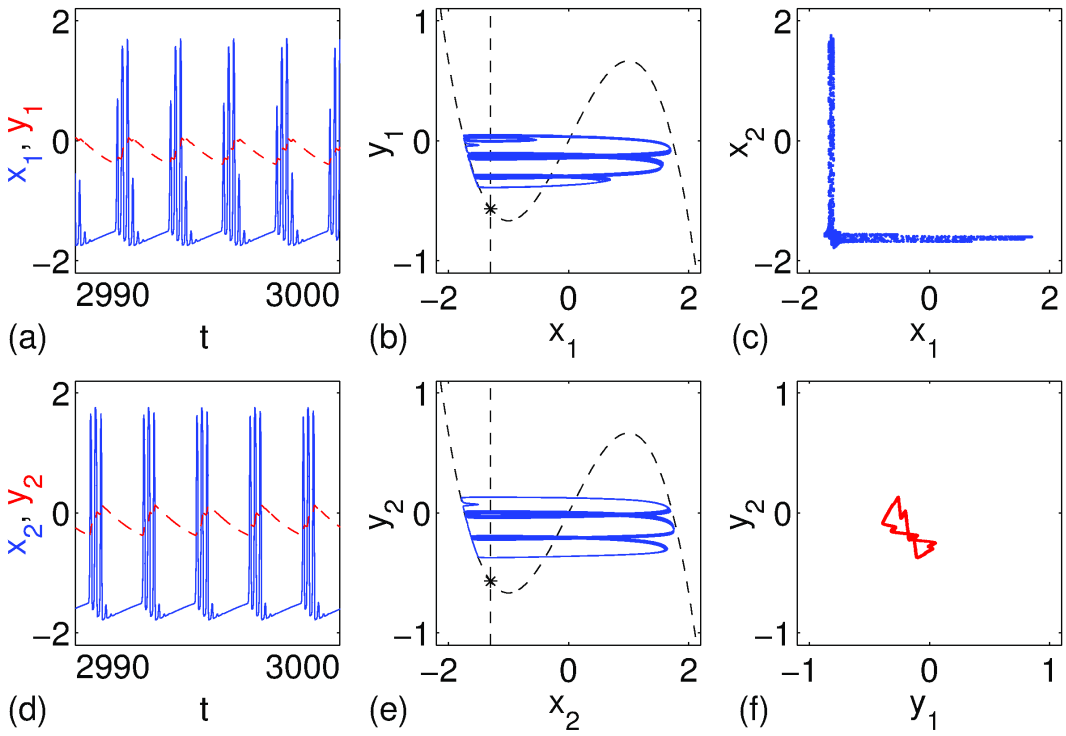


Fig. 13. Time series (a, d) and phase space projections (b, c, e, f) of x_1, y_1 and x_2, y_2 for the bursting-type solution of the system (2) with $K = 0.5, \tau_1^K = 2.2, \tau_2^K = 2$. Other parameters as in Fig. 2.

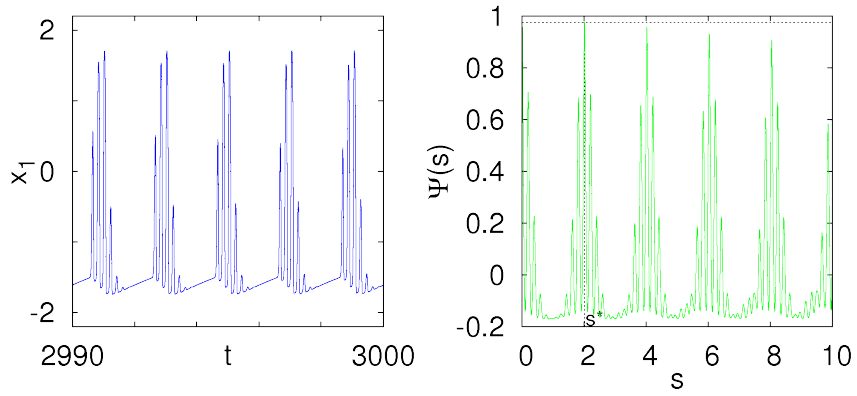


Fig. 14. (a) Time series of the first activator x_1 and (b) its autocorrelation function Ψ, for the same solution as in the Fig. 13. The dotted horizontal line in panel (b) refers to the chosen threshold for correlation detection. Other parameters as in Fig. 2.

on the basis of the mean interspike interval. For small feedback strengths, the system exhibits regular behavior with the period of about twice the mutual coupling delay. With increasing feedback strength, however, the self-feedback term becomes stronger and the system can perform more frequent spikes due to this additional source of excitation. This happens if the mutual coupling and self-feedback delays are in resonance. In the parameter plane of self-coupling delay and strength, the regions where the regular oscillations exist, resemble stripes emerging from the resonance with the mutual couping delays. We have provided an analytical formula for these resonance conditions and the period of the synchronized oscillations. A comparison with numerical simulations shows excellent agreement.

Next, we have focused on the case of non-identical self-coupling delays. We have considered two-dimensional projections of the parameter space and measured the regularity of the dynamics by the mean interspike interval as well as by the autocorrelation function. Similar to the case of identical self-coupling delays, we observe synchronized periodic dynamics, if the three delay times satisfy a resonance condition.

We have also derived a formula for the period of the synchronized regular dynamics, and compared the theoretical results with our numerical simulations.

Finally, we have studied bursts of subsequent excitation spikes. To identify such solutions the measure of interspike intervals is not appropriate any more, and we have used the autocorrelation function as an alternative tool for the analysis of the dynamics.

In conclusion, we have shown that heterogeneous time delays give rise to regular synchronization patterns of different periods, which depend upon resonance conditions of the involved time delays.

We have restricted our investigations to local dynamics of type-II excitability related to a Hopf bifurcation (FitzHugh-Nagumo model). It is also interesting to consider other models describing, for instance, type-I excitability involving a saddle-node bifurcation on an invariant cycle or physiologically oriented models such as Hodgkin-Huxley- or Morris-Lecar-like equations, but those studies are beyond the scope of the present paper. Another important direction for future research is to increase the number of elements. First approaches to study delayed coupling in large networks have already been reported (see references in Sec. 1). In principle, the results of the presented work can also be applied to coupled systems of more than two elements. Then one has to carefully analyze the combinatorics of the various exciting self-feedback and cross-coupling pluses based on the given network topology. In the case of networks, asymmetries in the coupling strengths can also become important, e.g., if multiple subthreshold excitations accumulate. In addition, different coupling strengths play a crucial role in the presence of both excitatory and inhibitory connections in neural networks. In the presented study of two coupled elements, however, incoming pulses result in all-or-nothing events: if the signal is large enough, it will trigger a full-scale excitation. Otherwise, only a small, subthreshold excitation is possible.

Acknowledgments

This work was partially supported by DFG in the framework of SFB 910. PH acknowledges support by the BMBF (grant no. 01GQ1001B). We thank Y. Maistrenko, W. Kinzel, I. Kanter, and M. Dahlem for valuable discussions.

Appendix A Approximation of the firing time

The formula (7b) was derived only for a close to unity, i.e., close to the bifurcation point. For larger values of a, however, a similar estimate holds. In fact, the idea is to integrate in time along the right branch of the cubic nullcline from the point B to the point C (See Fig. 4). If a is close to 1, the coordinates of these points can be approximated by $B(2, -2/3)$ and $C(1, 2/3)$. For large a this approximation is rather bad.

To improve the formula one can do the following. The x-coordinate of point A cannot exceed $-a$, because the cycle cannot cross the fixed point $P(-a, a^3/3 - a)$. Therefore, the maximum coordinates for A are approximately $(-a, a^3/3 - a)$. Since the transition from the left branch to the right branch of the cubic nullcline happens almost instantaneously, the y-coordinate of B could also be approximated as $a^3/3 - a$. This yields $B = (a/2 + \sqrt{12 - 3a^2}/2, a^3/3 - a)$.

To calculate the coordinates of the point C we proceed as follows. Since the periodic trajectory in Fig. 4(b) appears to be symmetric with respect to the origin $(0, 0)$, the y-coordinate of C can be obtained as $a - a^3/3$, and hence $C(a, a - a^3/3)$. This leads to the following improved approximation for the firing time T_f

$$T_f = \int_{x_B}^{x_C} \frac{1-x_1^2}{x_1+a} dx_1 \tag{A.1}$$

$$= \frac{x_B^2 - x_C^2}{2} - a(x_B - x_C) + (a^2-1)\ln\frac{x_B+a}{x_C+a} \tag{A.2}$$

$$= (a^2-1)\ln\frac{3a+\sqrt{12-3a^2}}{4a} - \frac{a}{4}\left(a+\sqrt{12-3a^2}\right) + \frac{3}{2}. \tag{A.3}$$

This yields a value of $T_f \approx 0.38$ for $a = 1.3$.

References

Adhikari, B. M., Prasad, A. & Dhamala, M. [2011] "Time-delay-induced phase-transition to synchrony in coupled bursting neurons," *Chaos* **21**, 023116.

Atay, F. M. (ed.) [2010] *Complex Time-Delay Systems*, Understanding Complex Systems (Springer, Berlin Heidelberg).

Atay, F. M., Jost, J. & Wende, A. [2004] "Delays, connection topology, and synchronization of coupled chaotic maps," *Phys. Rev. Lett.* **92**, 144101.

Balanov, A. G., Janson, N. B., Postnov, D. E. & Sosnovtseva, O. V. [2009] *Synchronization: From Simple to Complex* (Springer, Berlin).

Batista, C. A. S., Lopes, S. R., Viana, R. L. & Batista, A. M. [2010] "Delayed feedback control of bursting synchronization in a scale-free neuronal network," *Neural Networks* **23**, 114–124.

Boccaletti, S., Kurths, J., Osipov, G., Valladares, D. L. & Zhou, C. S. [2002] "The synchronization of chaotic systems," *Phys. Rep.* **366**, 1–101.

Brandstetter, S. A., Dahlem, M. A. & Schöll, E. [2010] "Interplay of time-delayed feedback control and temporally correlated noise in excitable systems," *Phil. Trans. R. Soc. A* **368**, 391–421.

Choe, C. U., Dahms, T., Hövel, P. & Schöll, E. [2010] "Controlling synchrony by delay coupling in networks: from in-phase to splay and cluster states," *Phys. Rev. E* **81**, 025205(R).

Choe, C. U., Flunkert, V., Hövel, P., Benner, H. & Schöll, E. [2007] "Conversion of stability in systems close to a Hopf bifurcation by time-delayed coupling," *Phys. Rev. E* **75**, 046206.

Dahlem, M. A., Hiller, G., Panchuk, A. & Schöll, E. [2009] "Dynamics of delay-coupled excitable neural systems," *International Journal of Bifurcation and Chaos* **19**, 745–753.

Dhamala, M., Jirsa, V. K. & Ding, M. [2004] "Enhancement of neural synchrony by time delay," *Phys. Rev. Lett.* **92**, 074104.

D'Huys, O., Fischer, I., Danckaert, J. & Vicente, R. [2011] "Role of delay for the symmetry in the dynamics of networks," *Phys. Rev. E* **83**, 046223.

D'Huys, O., Vicente, R., Erneux, T., Danckaert, J. & Fischer, I. [2008] "Synchronization properties of network motifs: Influence of coupling delay and symmetry," *Chaos* **18**, 037116.

Englert, A., Kinzel, W., Aviad, Y., Butkovski, M., Reidler, I., Zigzag, M., Kanter, I. & Rosenbluh, M. [2010] "Zero lag synchronization of chaotic systems with time delayed couplings," *Phys. Rev. Lett.* **104**, 114102.

Fiedler, B., Flunkert, V., Hövel, P. & Schöll, E. [2010] "Delay stabilization of periodic orbits in coupled oscillator systems," *Phil. Trans. R. Soc. A* **368**, 319–341.

FitzHugh, R. [1961] "Impulses and physiological states in theoretical models of nerve membrane," *Biophys. J.* **1**, 445–466.

Flunkert, V., D'Huys, O., Danckaert, J., Fischer, I. & Schöll, E. [2009] "Bubbling in delay-coupled lasers," *Phys. Rev. E* **79**, 065201(R).

Flunkert, V. & Schöll, E. [2012] "Chaos synchronization in networks of delay-coupled lasers: Role of the coupling phases," *New. J. Phys.* **14**, 033039.

Flunkert, V., Yanchuk, S., Dahms, T. & Schöll, E. [2010] "Synchronizing distant nodes: a universal classification of networks," *Phys. Rev. Lett.* **105**, 254101.

Friedrich, J. & Kinzel, W. [2009] "Dynamics of recurrent neural networks with delayed unreliable synapses: metastable clustering," *J. Comput. Neurosci.* **27**, 65–80.

Hauptmann, C., Omel'chenko, O. E., Popovych, O. V., Maistrenko, Y. L. & Tass, P. A. [2007] "Control of spatially patterned synchrony with multisite delayed feedback," *Phys. Rev. E* **76**, 066209.

Hauschildt, B., Janson, N. B., Balanov, A. G. & Schöll, E. [2006] "Noise-induced cooperative dynamics and its control in coupled neuron models," *Phys. Rev. E* **74**, 051906.

Heiligenthal, S., Dahms, T., Yanchuk, S., Jüngling, T., Flunkert, V., Kanter, I., Schöll, E. & Kinzel, W. [2011] "Strong and weak chaos in nonlinear networks with time-delayed couplings," *Phys. Rev. Lett.* **107**, 234102.

Hicke, K., D'Huys, O., Flunkert, V., Schöll, E., Danckaert, J. & Fischer, I. [2011] "Mismatch and synchronization: Influence of asymmetries in systems of two delay-coupled lasers," *Phys. Rev. E* **83**, 056211.

Hövel, P., Dahlem, M. A., Dahms, T., Hiller, G. & Schöll, E. [2009] "Time-delayed feedback control of delay-coupled neurosystems and lasers," *Preprints of the Second IFAC meeting related to analysis and control of chaotic systems (CHAOS09)* (World Scientific), (arXiv:0912.3395).

Hövel, P., Dahlem, M. A. & Schöll, E. [2010a] "Control of synchronization in coupled neural systems by time-delayed feedback," *International Journal of Bifurcation and Chaos* **20**, 813–815.

Hövel, P., Shah, S. A., Dahlem, M. A. & Schöll, E. [2010b] "Feedback-dependent control of stochastic synchronization in coupled neural systems," *From physics to control through an emergent view*, eds. Fortuna, L., Fradkov, A. L. & Frasca, M. (World Scientific, Singapore), pp. 35–44.

Just, W., Pelster, A., Schanz, M. & Schöll, E. [2010] "Delayed complex systems," *Theme Issue of Phil. Trans. R. Soc. A* **368**, pp.301-513.

Kanter, I., Kopelowitz, E., Vardi, R., Zigzag, M., Kinzel, W., Abeles, M. & Cohen, D. [2011] "Nonlocal mechanism for cluster synchronization in neural circuits," *Europhys. Lett.* **93**, 66001.

Kinzel, W., Englert, A., Reents, G., Zigzag, M. & Kanter, I. [2009] "Synchronization of networks of chaotic units with time-delayed couplings," *Phys. Rev. E* **79**, 056207.

Kyrychko, Y. N., Blyuss, K. B. & Schöll, E. [2011] "Amplitude death in systems of coupled oscillators with distributed-delay coupling," *Eur. Phys. J. B* **84**, 307–315.

Lehnert, J., Dahms, T., Hövel, P. & Schöll, E. [2011a] "Loss of synchronization in complex neural networks with delay," *Europhys. Lett.* **96**, 60013.

Lehnert, J., Hövel, P., Flunkert, V., Guzenko, P. Y., Fradkov, A. L. & Schöll, E. [2011b] "Adaptive tuning of feedback gain in time-delayed feedback control," *Chaos* **21**, 043111.

Liang, X., Tang, M., Dhamala, M. & Liu, Z. [2009] "Phase synchronization of inhibitory bursting neurons induced by distributed time delays in chemical coupling," *Phys. Rev. E* **80**, 066202.

Masoller, C., Torrent, M. C. & García-Ojalvo, J. [2008] "Interplay of subthreshold activity, time-delayed feedback, and noise on neuronal firing patterns," *Phys. Rev. E* **78**, 041907.

Masoller, C., Torrent, M. C. & García-Ojalvo, J. [2009] "Dynamics of globally delay-coupled neurons displaying subthreshold oscillations," *Philosophical Transactions of the Royal Society A: Mathematical, Physical and Engineering Sciences* **367**, 3255–3266.

Mosekilde, E., Maistrenko, Y. L. & Postnov, D. [2002] *Chaotic Synchronization: Applications to Living Systems* (World Scientific, Singapore).

Nagumo, J., Arimoto, S. & Yoshizawa., S. [1962] "An active pulse transmission line simulating nerve axon." *Proc. IRE* **50**, 2061–2070.

Panchuk, A., Dahlem, M. A. & Schöll, E. [2009] "Regular spiking in asymmetrically delay-coupled FitzHugh-Nagumo systems," *Proc. NDES 09* , 177–179arXiv:0911.2071v1.

Pikovsky, A. S., Rosenblum, M. G. & Kurths, J. [2001] *Synchronization, A Universal Concept in Nonlinear Sciences* (Cambridge University Press, Cambridge).

Popovych, O. V., Yanchuk, S. & Tass, P. A. [2011] "Delay- and coupling-induced firing patterns in oscillatory neural loops," *Phys. Rev. Lett.* **107**, 228102.

Pyragas, K. [1992] "Continuous control of chaos by self-controlling feedback," *Phys. Lett. A* **170**, 421.

Rosin, D. P., Callan, K. E., Gauthier, D. J. & Schöll, E. [2011] "Pulse-train solutions and excitability in an optoelectronic oscillator," *Europhys. Lett.* **96**, 34001.

Rossoni, E., Chen, Y., Ding, M. & Feng, J. [2005] "Stability of synchronous oscillations in a system of Hodgkin-Huxley neurons with delayed diffusive and pulsed coupling," *Phys. Rev. E* **71**, 061904.

Schöll, E., Hiller, G., Hövel, P. & Dahlem, M. A. [2009] "Time-delayed feedback in neurosystems," *Phil. Trans. R. Soc. A* **367**, 1079–1096.

Schöll, E. & Schuster, H. G. (eds.) [2008] *Handbook of Chaos Control* (Wiley-VCH, Weinheim), second completely revised and enlarged edition.

Selivanov, A. A., Lehnert, J., Dahms, T., Hövel, P., Fradkov, A. L. & Schöll, E. [2012] "Adaptive synchronization in delay-coupled networks of Stuart-Landau oscillators," *Phys. Rev. E* **85**, 016201.

Senthilkumar, D. V., Kurths, J. & Lakshmanan, M. [2009] "Inverse synchronizations in coupled time-delay systems with inhibitory coupling," *Chaos: An Interdisciplinary Journal of Nonlinear Science* **19**, 023107.

Vicente, R., Gollo, L. L., Mirasso, C. R., Fischer, I. & Gordon, P. [2008] "Dynamical relaying can yield zero time lag neuronal synchrony despite long conduction delays," *Proc. Natl. Acad. Sci.* **105**, 17157.

Wang, Q., Chen, G. & Perc, M. [2011a] "Synchronous bursts on scale-free neuronal networks with attractive and repulsive coupling," *PLoS ONE* **6**, e15851.

Wang, Q., Duan, Z., Perc, M. & Chen, G. [2008a] "Synchronization transitions on small-world neuronal networks: Effects of information transmission delay and rewiring probability," *EPL* **83**, 50008.

Wang, Q., Lu, Q. & Chen, G. [2008b] "Synchronization transition induced by synaptic delay in coupled fast-spiking neurons," *International Journal of Bifurcation and Chaos* **18**, 1189.

Wang, Q., Lu, Q., Chen, G., Feng, Z. & Duan, L. [2009a] "Bifurcation and synchronization of synaptically coupled FHN models with time delay," *Chaos, Solitons and Fractals* **39**, 918–925.

Wang, Q., Perc, M., Duan, Z. & Chen, G. [2009b] "Synchronization transitions on scale-free neuronal networks due to finite information transmission delays," *Phys. Rev. E* **80**, 026206.

Wang, Q., Perc, M., Duan, Z. & Chen, G. [2010a] "Impact of delays and rewiring on the dynamics of small-world neuronal networks with two types of coupling," *Physica A* **389**, 3299–3306.

Wang, Q.-Y., Aleksandra, M., Matjaž, P. & Lu, Q.-S. [2011b] "Taming desynchronized bursting with delays in the macaque cortical network," *Chinese Physics B* **20**, 040504.

Wang, Q.-Y. & Lu, Q.-S. [2005] "Time delay-enhanced synchronization and regularization in two coupled chaotic neurons," *Chinese Physics Letters* **22**, 543.

Wang, Q. Y., Lu, Q. S. & Duan, Z. S. [2010b] "Adaptive lag synchronization in coupled chaotic systems with unidirectional delay feedback," *Int. J. Nonlin. Mech.* **45**, 640–646.

Zhang, W., Tang, Y., Fang, J.-a. & Zhu, W. [2011] "Exponential cluster synchronization of impulsive delayed genetic oscillators with external disturbances," *Chaos* **21**, 043137.

Zigzag, M., Butkovski, M., Englert, A., Kinzel, W. & Kanter, I. [2009] "Zero-lag synchronization of chaotic units with time-delayed couplings," *Europhys. Lett.* **85**, 60005.

Zou, W., Tang, Y., Li, L. & Kurths, J. [2012] "Oscillation death in asymmetrically delay-coupled oscillators," *Phys. Rev. E* **85**, 046206.

Zou, W. & Zhan, M. [2009] "Partial time-delay coupling enlarges death island of coupled oscillators," *Phys. Rev. E* **80**, 065204.